Cancer Cell
Article

Oncogenic Braf Induces Melanocyte Senescence and Melanoma in Mice

Nathalie Dhomen,[1,5] Jorge S. Reis-Filho,[2,5] Silvy da Rocha Dias,[1,5] Robert Hayward,[1] Kay Savage,[2] Veronique Delmas,[3] Lionel Larue,[3] Catrin Pritchard,[4] and Richard Marais[1,*]
[1]Signal Transduction Team, Cancer Research UK Centre for Cell and Molecular Biology
[2]Breakthrough Breast Cancer Research Centre
The Institute of Cancer Research, London SW3 6JB, UK
[3]Institut Curie, UMR146 CNRS, 91405 Orsay, France
[4]Department of Biochemistry, University of Leicester, Leicester LE1 7RH, UK
[5]These authors contributed equally to this work
*Correspondence: rmarais@icr.ac.uk
DOI 10.1016/j.ccr.2009.02.022

SUMMARY

We show here that inducible expression of Braf^{V600E} off the endogenous *Braf* gene in mouse melanocytes stimulates skin hyperpigmentation and the appearance of nevi harboring senescent melanocytes. Additionally, approximately 70% of Braf^{V600E} mice develop melanomas that reproduce many of the cardinal histological and molecular features of human melanoma and whose cells can colonize the lungs of nude mice. We show that the tumor suppressor p16^{INK4a} is not required to induce melanocyte senescence and that its loss is not required for tumor progression, although it does regulate tumor penetrance and latency. Thus, we have developed a mouse model of melanoma driven by Braf^{V600E} expressed at physiological levels that reflects the genetics and pathology of the human disease.

INTRODUCTION

Melanoma is an aggressive form of skin cancer that arises from cells called melanocytes, specialized pigmented cells that provide skin tone, hair color, and protection from ultraviolet radiation. The serine/threonine-specific protein kinase BRAF, a component of the RAS/RAF/MEK/ERK signaling pathway, is a key player in melanoma because it is activated by somatic gain-of-function mutations in 50%–70% of human melanomas, making it the most frequently mutated oncogene in this disease (Garnett and Marais, 2004). A substitution of glutamic acid for valine at position 600 (V600E) is the most common mutation in BRAF in melanoma (occurring in over 90% of cases), and BRAF^{V600E} stimulates constitutive cell signaling, growth factor-independent proliferation, and transformation of immortalized melanocytes, allowing these cells to grow as tumors in nude mice (Hingorani et al., 2003; Hoeflich et al., 2006; Karasarides et al., 2004; Wellbrock et al., 2004). Inhibitors of BRAF^{V600E} signaling block melanoma cell proliferation and induce apoptosis in vitro; in vivo they slow the growth of melanoma xenografts. These data demonstrate that BRAF^{V600E} is necessary for the maintenance and progression of melanoma in humans.

Despite its clear association with tumor maintenance and progression, overexpression of BRAF^{V600E} in zebrafish melanocytes only induces nevus-like clusters of cells that do not progress to melanoma unless *p53* is also deleted (Patton et al., 2005). Furthermore, *BRAF^{V600E}* mutations are found in up to 80% of human nevi, benign melanocytic lesions that can remain unchanged for decades (Pollock et al., 2003), and BRAF^{V600E} induces classical oncogene-induced senescence in human melanocytes in vitro (Gray-Schopfer et al., 2006; Michaloglou et al., 2005). Together, these data indicate that BRAF^{V600E} is not sufficient for melanoma induction and that additional genetic or epigenetic changes are required to induce full melanocyte transformation. Furthermore, the data do not reveal whether *BRAF^{V600E}* is a founder, a driver, or a passenger mutation in melanomagenesis, a question that cannot be addressed using approaches that rely on transformation of immortalized

SIGNIFICANCE

BRAF is mutated in 50%–70% of human melanomas, and we have developed a mouse model of melanoma that is driven by Braf^{V600E}, the most common *BRAF* mutant found in the human disease. This model is important because it is driven by the most relevant human oncogene expressed at physiological levels. The close similarities between the tumors that develop in our mice and those seen in humans show that we can now dissect melanoma genetics and study its pathology in this highly tractable model system. Notably, our data establish that Braf^{V600E} can induce melanocyte senescence in vivo and that the acquisition of a *BRAF* mutation can be a founder event in melanomagenesis.

Table 1. Genotyping of Pups Resulting from Intercross between *Braf*$^{+/LSL\text{-}V600E}$ and *Tyr::CreERT2*$^{+/o}$ Mice

Genotype	Phenotype	Expected	Observed
Braf$^{+/+}$;*Tyr::CreERT2*$^{o/o}$	wild-type	25%	27% (102)
Braf$^{+/LSL\text{-}V600E}$; *Tyr::CreERT2*$^{o/o}$	Braf^{V600E}	25%	25% (93)
Braf$^{+/+}$;*Tyr::CreERT2*$^{+/o}$	CreERT2	25%	22% (82)
Braf$^{+/LSL\text{-}V600E}$; *Tyr::CreERT2*$^{+/o}$	Braf^{V600E}/CreERT2	25%	26% (99)

The expected and observed frequency of each genotype is shown as a percentage, with the absolute numbers of individuals shown in parentheses.

melanocytes in vitro or on the study of melanoma cells from patients with existing metastatic disease.

The purpose of this work was to develop a mouse model of melanoma driven by oncogenic Braf that would emulate the human disease. Specifically, we wished to mimic the acquisition of somatic *BRAF* mutations that occurs in human melanoma by expressing Braf^{V600E} in the melanocytes of postnatal mice using the endogenous *Braf* gene. Our aim was to determine whether expression of Braf^{V600E} at physiological levels could induce melanoma in mice, to use these mice to investigate the role of p16^{INK4a} in melanoma progression, and to determine whether the acquisition of a *Braf* mutation could be a founder mutation in melanoma.

RESULTS

To develop our mouse model of melanoma, we used a transgenic mouse strain (*LSL-Braf*^{V600E}) that we previously developed that allows inducible expression of Braf^{V600E} off the endogenous *Braf* gene using *LoxP*-stop-*LoxP* (LSL)/Cre recombinase technology (see Figure S1 available online; Mercer et al., 2005). *Braf*^{V600E} expression from this locus is normally suppressed by the presence of a minigene encoding wild-type Braf and the Neo^{R} cassette used for embryonic stem cell selection. However, expression can be induced when the locus is rearranged by Cre recombinase. To regulate the rearrangement of the *LSL-Braf*^{V600E} locus, a tamoxifen (TM)-activated version of Cre recombinase (CreERT2; Indra et al., 1999) was placed under the control of a tyrosinase enhancer/promoter construct (Yajima et al., 2006), allowing precise control of Braf^{V600E} expression in melanocytes in postnatal mice. Since Braf^{V600E} is expressed off the endogenous gene and expression can be regulated by TM treatment, this approach closely mimics the somatic acquisition of *BRAF* mutations that occurs in human melanoma. *LSL-Braf*^{V600E} mice were crossed to *Tyr::CreERT2*$^{+/o}$ mice, and double-targeted *LSL-Braf*^{V600E};*Tyr::CreERT2*$^{+/o}$ (hereafter referred to as *Braf*^{V600E}/*CreERT2*) mice were obtained at the expected Mendelian ratio (Table 1). The untreated double-targeted mice appeared normal, were fertile, and exhibited a normal life span (data not shown).

To induce Braf^{V600E} expression, TM was applied to the shaven skin on backs of the mice 2–3 months after birth. Two TM treatment schedules (8 treatments over 8 days versus 4 treatments over 7 days) at two doses (20 mg versus 1 mg) were tested, and within 2 months, the *Braf*^{V600E}/*CreERT2* mice developed skin hyperpigmentation independently of the treatment schedule used. Their snouts, tails, ears, and paws all darkened visibly (Figures 1A–1D). This systemic effect was unexpected because TM was only applied to a small section of skin on the backs of the mice (approximately 1 cm^2) and suggests that TM was absorbed into the circulation through the dermis or was ingested during grooming after treatment. Skin hyperpigmentation due to increased melanocyte proliferation is also seen when Hras^{G12V} or Nras^{Q61K} is overexpressed using melanocyte-specific promoters (Ackermann et al., 2005; Powell et al., 1995), but we also observed less penetrant phenotypes,

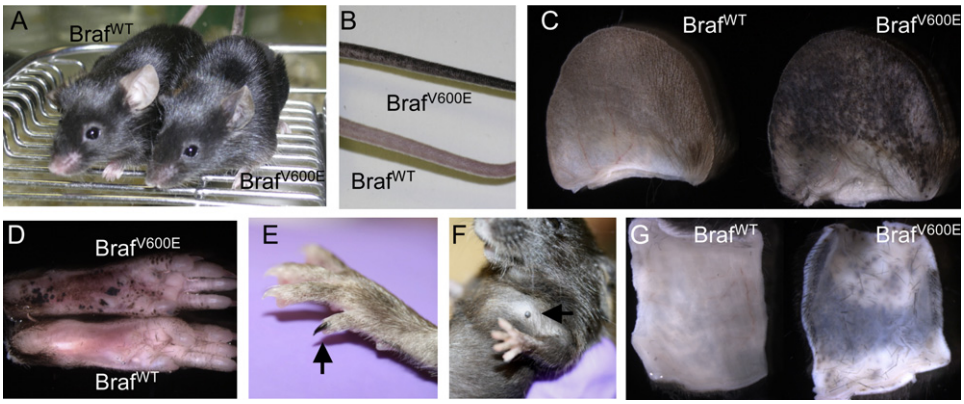

Figure 1. Phenotype of Braf^{V600E}-Expressing Mice

The comparison shown here is between tamoxifen (TM)-treated Braf^{WT} (*Braf*$^{+/+}$;*Tyr::CreERT2*$^{+/o}$) and Braf^{V600E} (*LSL-Braf*^{V600E};*Tyr::CreERT2*$^{+/o}$) mice.
(A) Braf^{WT} and Braf^{V600E} siblings.
(B) Tails of Braf^{WT} and Braf^{V600E} mice.
(C) Ears of Braf^{WT} and Braf^{V600E} mice.
(D) Feet of Braf^{WT} and Braf^{V600E} mice.
(E) Proximal toenail of the right hind foot of a Braf^{V600E} mouse (arrow).
(F) Anterior nipple of a Braf^{V600E} female mouse (arrow).
(G) Skin from the inside of Braf^{WT} and Braf^{V600E} mice.

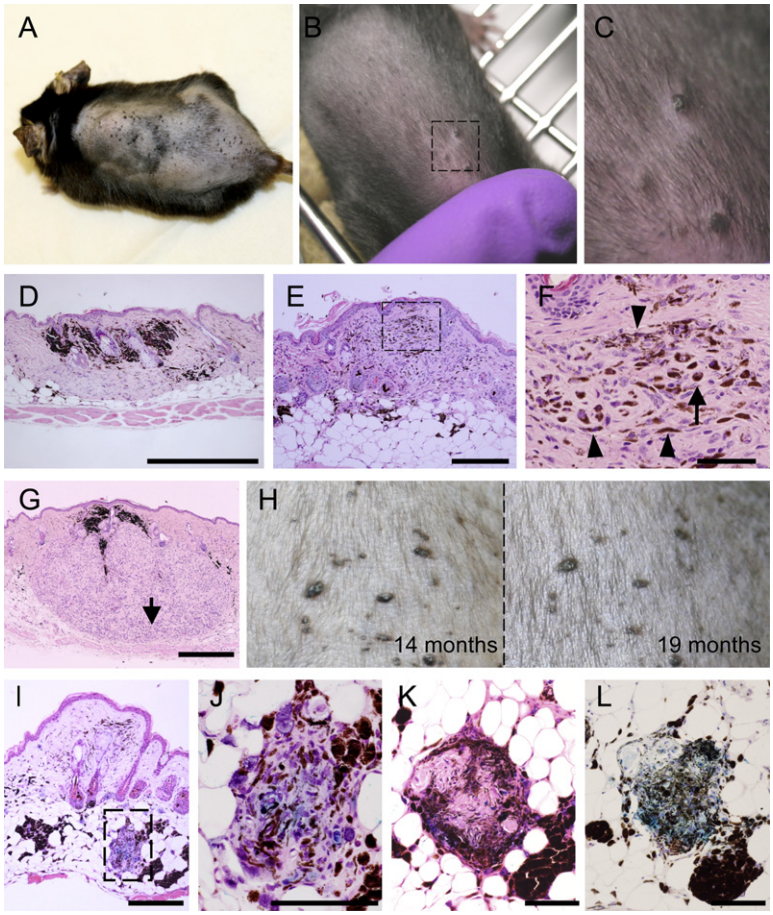

Figure 2. $Braf^{V600E}$ Induces Nevi in Mice

(A) Photograph of the back of a $Braf^{V600E}$ mouse after treatment with four 20 mg doses of TM. The fur has been removed to reveal the nevi.

(B) Photograph of the back of a $Braf^{V600E}$ mouse after treatment with four 1 mg doses of TM. The fur has been removed to reveal the nevi.

(C) Enlargement of the region indicated in (B).

(D–G) Photomicrographs of nevi from the backs of TM-treated $Braf^{V600E}$ mice. The indicated region in (E) is magnified in (F) and shows the presence of epithelioid (arrow) and spindle dendritic (arrowheads) cells. (G) shows a symmetrical lesion with pushing borders displaying an area of unpigmented differentiated cells resembling a hypopigmented blue nevus (Carr et al., 1997). Scale bars = 500 μm in (D), (E), and (G); 100 μm in (F).

(H) Photographs of the TM-treated area of a $Braf^{V600E}$ mouse taken 14 and 19 months after TM treatment.

(I and J) Sections of a nevus stained for hematoxylin and eosin and senescence-associated (SA)-β-galactosidase (light blue). The indicated region in (I) is magnified in (J). Note the expression of SA-β-galactosidase in melanocytic cells. Scale bars = 500 μm in (I); 100 μm in (J).

(K and L) Deeper aspect of a nevus where melanocytic cells are encasing a nerve bundle. The neoplastic cells express SA-β-galactosidase (light blue) and fail to display Ki-67 nuclear staining (DAB/brown; similar results were observed with other chromogens, including AEC). Note the presence of a cluster of melanophages in the bottom right corner. Scale bars = 100 μm.

including darkening of the toenails proximal to the body on the front and/or hind feet (equivalent to human thumbs or big toes; Figure 1E) in 40% of the animals and darkening of anterior nipples (Figure 1F) in ~50% of the females. The hairy skin also darkened, visible most clearly when examined from the inside and generally only within the TM-treated areas (Figure 1G). No such phenotypes were observed in ethanol-treated *$Braf^{V600E}$/CreERT2* mice or in TM-treated controls that included *LSL-$Braf^{V600E}$*- and *Tyr::CreERT2*-only targeted mice (Figure 1 and data not shown).

$Braf^{V600E}$ expression also induced nevi in all of the animals (Figures 2A–2C). These were most abundant in the TM-treated areas but occasionally appeared in untreated areas such as the ears and belly (data not shown). They were more widespread on mice treated with high doses of TM (compare Figure 2A and Figure 2B) and were not seen in ethanol-treated *$Braf^{V600E}$/CreERT2* controls or other TM-treated mice. The nevi appeared as pigmented dome-shaped outgrowths in the dermis (Figure 2C). They were never located in the epidermis and did not possess a junctional (epidermal/dermal crossover) component (Figures 2D and 2E). These lesions were composed of pigmented epithelioid or dendritic melanocytes (arrow and arrowheads, respectively, in Figure 2F). Neuroid differentiation, producing regions of unpigmented cells, occurred below the nevus in some cases, and a clearly defined border was still evident (Figure 2G). The histopathological features of these lesions were consistent with those of human blue nevi. These nevi did not undergo obvious changes in morphology or pigmentation over extended periods of the life span of the mice (Figure 2H), and they stained positive for senescence-associated (SA)-β-galactosidase, particularly in their deeper aspects (Figures 2I–2L). The absence of mitotic figures (data not shown) and lack of staining for the proliferation marker Ki-67 (Figure 2L) demonstrated that these lesions possessed low levels of cell proliferation.

$Braf^{V600E}$ also induced large melanocytic lesions around the perianal regions and in the eyelids of the mice (Figures 3A and 3B). Multiple blue nevi as described above were often adjacent to, but not contiguous with, these lesions. Those in the eyelids arose 3–5 months after $Braf^{V600E}$ expression and occurred in 80% of animals, whereas the perianal lesions appeared after 6–10 months and generally only in the animals treated with high doses of TM. These lesions (anal lesions, Figures 3C–3E; eyelid lesions, Figures 3F and 3G) were dome-shaped and composed of a complex mixture of heavily pigmented epithelioid cells (Figure 3D, white arrowheads), which dominated the central aspects, and spindle melanocytic cells (Figure 3D, black arrowheads), which predominated at the periphery. The large, epithelioid-shaped melanocytes were admixed with less densely pigmented epithelioid melanocytes and melanophages. The neoplastic cells contained uniform, round nuclei, with vesicular chromatin and small but discrete nucleoli (Figure 3H). In the

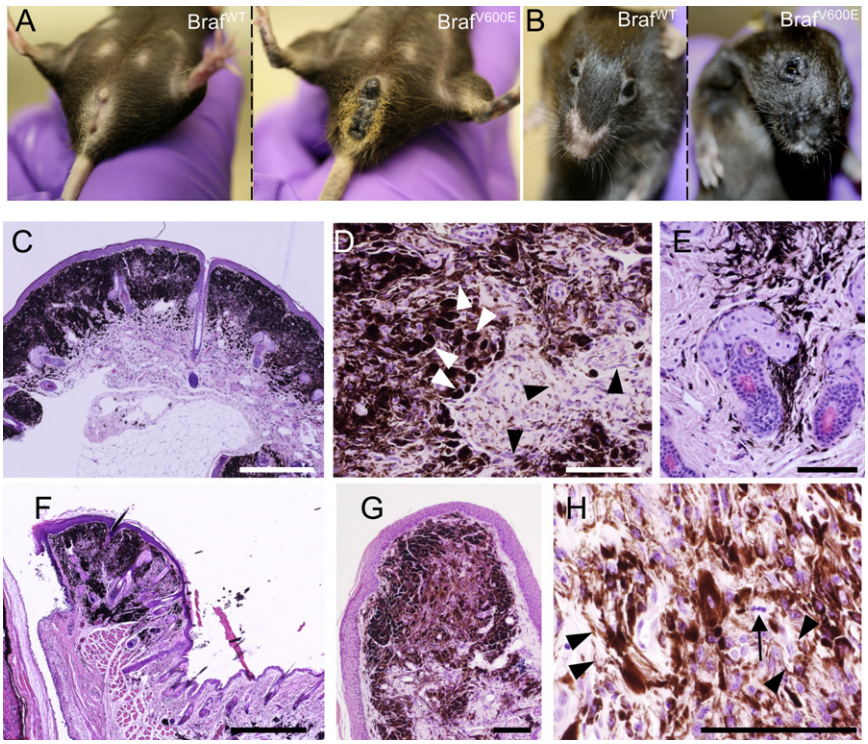

Figure 3. Braf^{V600E} Induces Epithelioid Blue Nevi

(A) Photograph showing large pigmented perianal lesion in a Braf^{V600E}-expressing mouse treated with four 20 mg doses of TM (right), compared to a Braf^{WT} control mouse (left).

(B) Photograph showing melanocytic lesions in the eyelids of a Braf^{V600E} expressing mouse treated with four 20 mg doses of TM (right), compared to a similarly treated Braf^{WT} mouse (left).

(C) Photomicrograph of a section from a large pigmented perianal epithelioid blue nevus stained with hematoxylin and eosin. Scale bar = 500 μm.

(D) Photomicrograph of a magnified region of an epithelioid blue nevus displaying large heavily and lightly pigmented epithelioid melanocytic cells (white arrowheads) and a small number of lightly pigmented spindle-shaped melanocytes (black arrowheads), occasionally with dendritic projections. Scale bar = 100 μm.

(E) Photomicrograph of an epithelioid blue nevus showing dendritic cells extending along the periadnexal structures of the skin. Scale bar = 100 μm.

(F and G) Low-power magnification of epithelioid blue nevi of the eyelid. Note the presence of epidermal hyperplasia and that the lesion is composed of epithelioid cells with varying degrees of pigmentation and spindle cells. Scale bars = 500 μm in (F); 100 μm in (G).

(H) High-power magnification of an epithelioid blue nevus composed of spindle (arrowheads) and epithelioid cells. Note the presence of a mitotic figure (arrow). Scale bar = 100 μm.

epithelioid cells, the cytoplasm was abundant and heavily melanin laden (Figures 3C, 3D, 3F, and 3G). Heavily pigmented cells could be found throughout the lesions, including at the base (Figures 3C, 3F, and 3G). A small number of lightly pigmented spindle-shaped melanocytes with poorly defined cell borders were also observed (Figures 3D and 3H; black arrowheads). Many of these cells were arranged either haphazardly or in short fascicles. The spindle cells often displayed dendritic extensions (Figures 3E and 3H) and spread to the subcutaneous adipose tissue along the periadnexal connective tissue of the hair follicles, pilar muscle, eccrine coils, or neovascular bundles (Figures 3C and 3E–3G). As with the ordinary blue nevi, these lesions were largely restricted to the dermal layers of the skin, and epidermal hyperplasia was observed (Figures 3C, 3F, and 3G). Rare mitotic figures (one mitosis in 30 high-power fields; Figure 3H, arrow) were seen, but never at the base of the lesions. These histological features are consistent with a diagnosis of epithelioid blue nevus, originally described in patients with Carney complex but also found as sporadic solitary lesions (Moreno et al., 2000; Zembowicz et al., 2004). It has been suggested that epithelioid blue nevi are variants of blue nevi (Groben et al., 2000), and the coexistence of both blue nevi and epithelioid blue nevi in our mice is consistent with this hypothesis. Furthermore, as in the mice described here, epithelioid blue nevi have also been observed to arise in genital mucosal areas in humans (Izquierdo et al., 2001).

Braf^{V600E} also induced rapidly growing hypopigmented tumors in 60%–70% of the mice (Figure 4A). These were asymmetrical and displayed an overt locally destructive growth pattern (Figure 4B; Figures S2A and S2B). Remnants of blue nevi that were contiguous with the tumors were seen occasionally (Figure 4C, arrowheads), and no junctional components were found. These poorly circumscribed lesions were centered at the superficial dermis, often (38%) ulcerated the overlying epidermis (Figures 4B and 4C; Figures S2C and S2D), and infiltrated the subcutis, skeletal muscle, and auricular cartilage in a destructive fashion (Figures 4B, 4J, and 4K; Figures S2A and S2B). The tumors were composed of a mixture of (1) atypical spindle and plump spindle cells either arranged in short fascicles (Figure 4D; Figures S2E and S2F) occasionally in storiform pattern or immersed in a myxoid matrix and (2) discohesive atypical epithelioid cells (Figures 4E–4G; Figures S2G and S2H), with pleomorphic nuclei containing conspicuous nucleoli (Figure 4E–4G), that were either isolated or vaguely arranged into nests (Figure 4E–4I). Although no lymphocytic infiltrate or pagetoid cells were found, these lesions displayed several histological and cytological features of cells usually found in malignant melanomas: increased nuclear/cytoplasmic ratios (Figures 4F and 4G) together with atypical and pleomorphic nuclei (Figures 4E–4G and 4J) and numerous nuclear pseudoinclusions (Figures 4D, 4F, 4H, and 4I, arrows). Rare, morphologically unequivocal neoplastic cells containing dusty brownish cytoplasmic pigment (Figures 4D and 4G) that were positive for Masson-Fontana stain (data not shown) were observed, and abundant mast cells were also present throughout the lesions. Areas of necrosis within the tumor bulk were often observed (Figure S2D). Clusters of melanophages, mostly restricted to the superficial aspects of the lesions, were also often found (data not shown). Additionally,

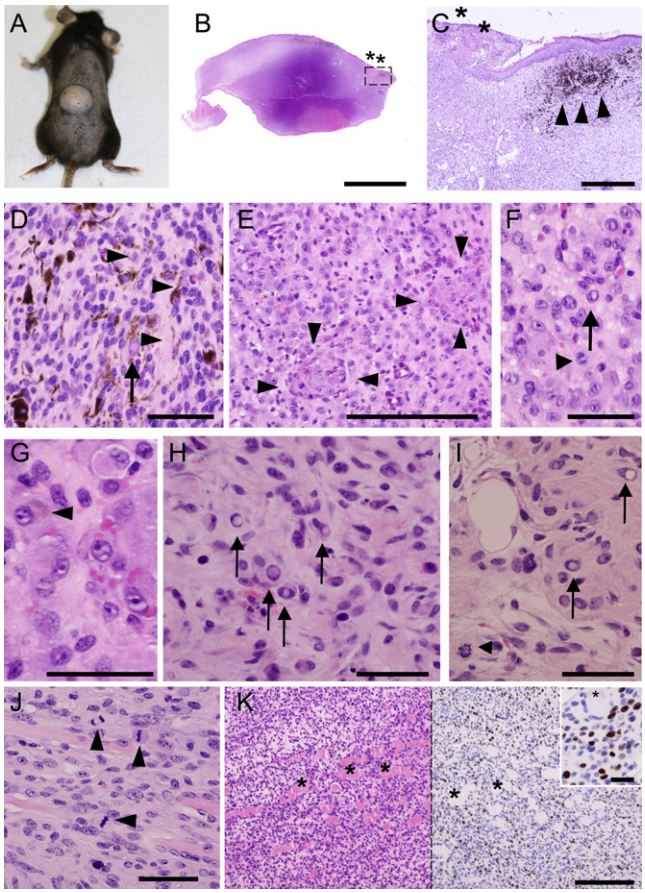

Figure 4. $Braf^{V600E}$ Induces Melanoma in Mice

(A) Photograph showing a large hypopigmented tumor on a TM-treated $Braf^{V600E}$ mouse. The fur has been removed to reveal the lesion.

(B) Scanning magnification of an oligomelanotic malignant melanoma demonstrating its asymmetry, destructive growth pattern, and ulceration. Scale bar = 0.5 cm.

(C) High-power magnification of the region indicated in (B) of a $Braf^{V600E}$-induced tumor showing remnants of a nevus at its periphery (arrowheads) and ulceration. Scale bar = 200 μm.

(D) Deep area composed predominantly of spindle cells, some of which harbor nuclear pseudoinclusions (arrow). Note the presence of numerous pigmented spindle cells with long dendritic cytoplasmic projections (arrowheads). Scale bar = 50 μm.

(E) Discohesive epithelioid neoplastic cells are occasionally arranged in a vaguely nested pattern (arrowheads). Scale bar = 200 μm.

(F and G) Atypical epithelioid neoplastic cells displaying increased nuclear cytoplasmic ratios and pleomorphic nuclei with conspicuous nucleoli. Rare rhabdoid cells could also be found. Note the presence of nuclear pseudoinclusions (arrow in [F]) and cells with dusty, intracytoplasmic brown pigment (arrowhead in [G]). A mitotic figure is also indicated in (F) (arrowhead). Scale bars = 50 μm.

(H) Neoplastic cells displaying numerous nuclear pseudoinclusions (arrows). Scale bar = 50 μm.

(I) Neoplastic cells arranged in a vaguely nested pattern displaying numerous nuclear pseudoinclusions (arrows). Note the presence of a mitotic figure (arrowhead). Scale bar = 50 μm.

(J) Deep area of an oligomelanotic melanoma composed of spindle cells infiltrating the skeletal muscle. Note the presence of numerous mitotic figures (arrowheads). Scale bar = 50 μm.

(K) Left: deep area of a predominantly spindle cell malignant melanoma infiltrating the skeletal muscle. Right: serial section subjected to immunohistochemical analysis with antibodies against Ki-67 (MIB1) highlighting the presence of proliferating cells in deep areas. Inset: Ki-67-positive neoplastic cells. Note the residual skeletal muscle fiber. Scale bars = 200 μm in main figure; 50 μm in inset.

these lesions typically showed significantly increased levels of mitotic activity compared to nevi. Mitotic figures, which were extremely rare in the nevi (Figure 3H), were common in the tumors (Figures 4F, 4I, and 4J, arrowheads), with an average mitotic index of 11 mitoses/10 high-power fields (10 tumors analyzed). Mitotic figures were observed in both the superficial and deep aspects of the lesions (Figure 4J), and atypical mitotic figures were readily observed. Ki-67 labeling indices ranged from 11% to 28%, and Ki-67-positive nuclei were present throughout the lesions, including within their deep aspects (Figure 4K).

Positive immunoreactivity for S100, a common marker for melanoma (Ohsie et al., 2008), was observed in all tumors (Figures 5A and 5B). Interestingly, even the lesions composed predominantly of spindle cells arranged in storiform pattern were diffusely positive for S100, suggesting that these tumors were not malignant peripheral nerve sheath tumors (King et al., 1999). In addition to S100, antibodies to HMB45 (gp100), MART-1, and MITF were also tested, but these failed to consistently stain melanocytes in fixed mouse skin sections and did not consistently stain mouse B16 melanoma cells fixed according to the same protocol (data not shown). The vast majority of neoplastic cells were highly atypical, lacked pigmentation, and were poorly differentiated, which may also have contributed to the difficulty encountered in the immunohistochemical analysis. To circumvent the lack of adequate reagents for immunohistochemical analysis, we used alternative approaches to examine the lesions for expression of melanocytic lineage genes and melanoma markers. First, we showed that all tumors displayed evidence of *LSL-$Braf^{V600E}$* locus recombination (Figure 5C). Then, we used RT-PCR to show evidence of tyrosinase, Trp2, Pax3, and Silver (the mouse equivalent of gp100) expression (Figure 5D) in the amelanotic/oligomelanotic malignant lesions.

We hypothesized that the neoplastic cells in the amelanotic/oligomelanotic malignant lesions were either undifferentiated or poorly differentiated and of melanocytic origin. To test this, we generated clonal cell lines from the primary tumors and treated them with cholera toxin, a known inducer of melanocyte differentiation (O'Keefe and Cuatrecasas, 1974). Notably, the clonal lines constitutively expressed the melanocytic markers *tyrosinase*, *Trp2*, and *Silver*, but the levels of expression of these genes were markedly increased when cells were treated with cholera toxin (Figure S3A). Furthermore, cholera toxin induced the tumor cells to adopt a more differentiated, dendritic morphology (Figure S3B). Together with the histological, immunohistochemical, and RT-PCR results, these findings provide strong circumstantial evidence suggesting that the lesions we observed are oligomelanotic malignant melanomas.

We did not observe any examples of metastatic tumor growth, although 38% of lesions were ulcerated (Figures 4B and 4C; Figures S2C and S2D) and neoplastic cells displayed overt destructive growth destroying subjacent subcutaneous tissues, skeletal muscle, and, when the lesions affected the ears, the auricular cartilage (Figures S2A and S2B). In human pathology, these are diagnostic features used to differentiate malignant

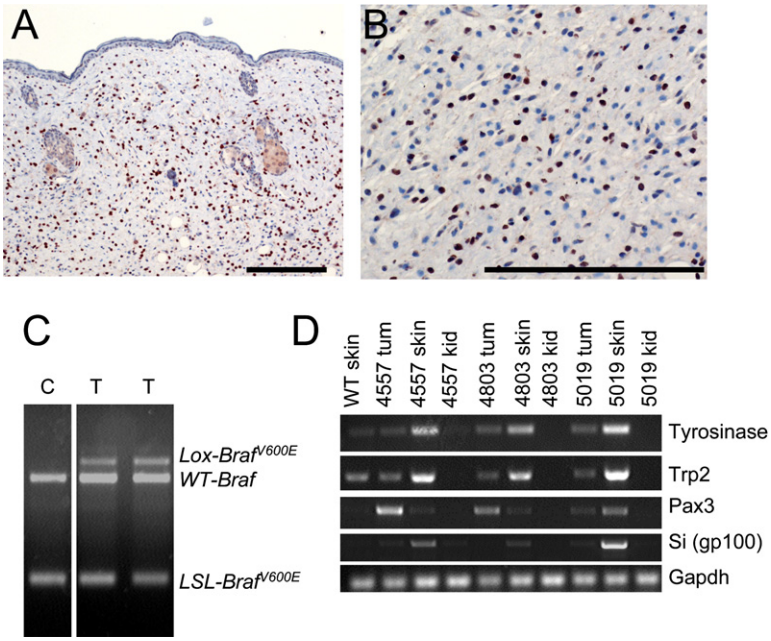

Figure 5. TM-Treated Braf^{V600E} Mice Develop Malignant Tumors that Have Features of Melanocytic Differentiation

(A and B) Low- and high-power micrographs of a spindle cell lesion expressing S100 protein in the nuclei of the vast majority of neoplastic cells. Immunohistochemistry was performed with polyclonal anti-S100 protein antibody (avidin-biotin-peroxidase/DAB). Scale bars = 200 μm.

(C) PCR-mediated genotyping of the *Braf* alleles in DNA extracted from tumors (T) or from the skin of untreated control (C) mice. The positions of wild-type *Braf* (*WT-Braf*), the *LSL-Braf^{V600E}* allele, and the Cre recombinase-rearranged *LSL-Braf^{V600E}* locus (*Lox-Braf^{V600E}*) are indicated.

(D) Expression of the melanoma markers *tyrosinase*, *Trp2*, *Pax3*, and *Silver* (*Si*) in tumors (tum) of TM-treated Braf^{V600E} mice. RNA from melanocyte-rich ear skin (skin) from a wild-type mouse was used as a positive control. DNA from the kidneys (kid) was used as a negative control. Numbers refer to individual mice.

from benign melanocytic lesions. Therefore, to test whether neoplastic cells from these lesions have metastatic potential, tumor cells were harvested for in vitro culture, engineered to express firefly luciferase, and injected into the tail veins of nude mice. Using intravital imaging, the cells were shown to colonize the lungs in all (15 of 15) of the recipient mice (Figure 6A). Postmortem examination revealed that the lungs contained multiple tumor foci and were significantly heavier than lungs from PBS-injected controls (Figures 6B and 6C). The metastatic deposits contained neoplastic cells whose morphology resembled that of cells in the primary tumors (Figure 6D).

Previous studies have shown that Nras^{Q61K} induces metastatic melanoma in *p16^{INK4a}* null mice (Ackermann et al., 2005), so we examined whether Braf^{V600E} could also stimulate metastatic melanomas in *p16^{INK4a}* null animals by crossing the *Braf^{V600E}/CreERT2* mice onto a *p16^{INK4a}* null background (note that these mice still express *p19^{Arf}* [Krimpenfort et al., 2001]). In the wild-type *p16^{INK4a}* background, Braf^{V600E} induced melanoma in 54% of the mice within 12 months, increasing to 64% after 14 months and a median latency of 12 months (Figure 6E). Tumors did not develop in vehicle-treated *Braf^{V600E}/CreERT2* mice or in TM-treated controls (Figure 6E; Table 2). However, in the *p16^{INK4a}* null background, 80% of the mice developed tumors within 12 months, and the latency dropped to 7 months (Figure 6E). In addition, while wild-type *p16^{INK4a}* animals tended to develop only single tumors, the *p16^{INK4a}* null mice generally developed multiple tumors (data not shown). Surprisingly, the *p16^{INK4a}* null mice still developed nevi (Figure 6F), and the nevi and tumors of wild-type *p16^{INK4a}* mice still expressed *p16^{INK4a}* mRNA (Figure 6G). We sequenced the *p16^{INK4a}* mRNA from the tumors and did not detect any mutations within its open reading frame (data not shown). Commensurate with this, we demonstrated that p16^{INK4a} protein was expressed in the nuclei of melanomas from wild-type *p16^{INK4a}* animals (Figure 6H), suggesting that the protein is active. As a control for the p16^{INK4a} staining, we demonstrated that there was no specific staining for this protein in tumors from *p16^{INK4a}* null mice (Figure 6H).

DISCUSSION

In this study, we show that Braf^{V600E} expression induces several types of melanocytic lesions in mice, including skin hyperpigmentation, benign classic and epithelioid blue nevi, and melanoma. Nevi and melanoma are genetically linked because individuals from melanoma-susceptible families have unusually high numbers of nevi (Hayward, 2000), but the relationship between BRAF, nevi, and melanoma is unclear because *BRAF* mutations are as common in nevi as they are in melanoma (Pollock et al., 2003). Furthermore, whereas BRAF^{V600E} stimulates melanoma cell proliferation, it induces senescence in melanocytes (Garnett and Marais, 2004; Gray-Schopfer et al., 2006; Michaloglou et al., 2005; Pollock et al., 2003). Overexpressed Hras^{G12V} can induce nevi in mice, but the animals do not develop melanoma unless tumor suppressor genes such as *p16^{INK4a}* or *p19^{Arf}* are also deleted (Ackermann et al., 2005; Chin et al., 1997, 1999; Huijbers et al., 2006; Powell et al., 1995) or the animals are treated with carcinogens such as DMBA or ultraviolet radiation (Broome Powell et al., 1999; Kannan et al., 2003). Additionally, although Nras^{Q61K} induces melanoma in *p16^{INK4a}* null mice, it does not induce nevi (Ackermann et al., 2005).

Thus, unlike oncogenic Ras, Braf^{V600E} can induce both melanocyte senescence and melanoma in mice, and it does so without the need for additional manipulation of the genome. Furthermore, Braf^{V600E} was expressed off the endogenous *Braf* gene and balanced over a wild-type allele, and it therefore closely mimics the genetics of the human disease. We have previously shown that BRAF^{V600E} transforms immortalized melanocytes (Wellbrock et al., 2004), but these results are important because they establish that Braf^{V600E} can be a founder event in melanomagenesis and are consistent with a model whereby Braf^{V600E} stimulates melanocytic proliferation but cannot induce

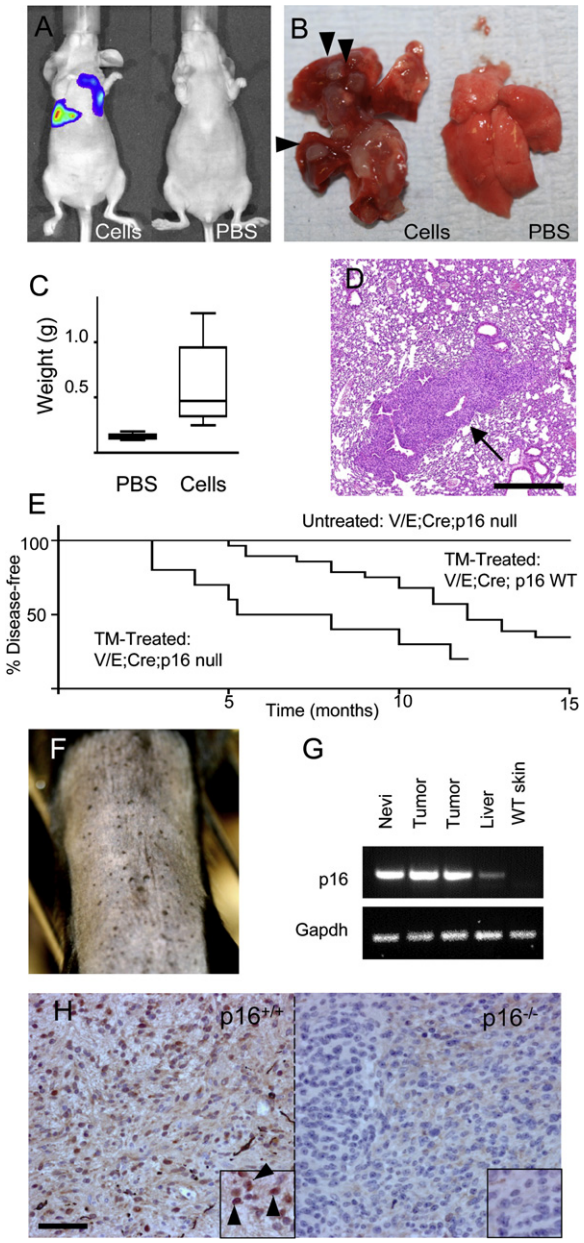

Figure 6. Metastatic Potential and p16 Status of Braf^{V600E} Tumors

(A) Intravital imaging of mice injected with 3 × 10^5 luciferase-expressing Braf^{V600E}-induced melanoma cells (left) or with PBS (right) in the tail vein. The image was captured 31 days postinjection.

(B) Lungs from mice injected with 3 × 10^5 luciferase-expressing Braf^{V600E}-induced melanoma cells (left) or with PBS (right) in the tail vein. Tumor nodules are indicated by arrowheads.

(C) Box plot of lung weights from mice injected with PBS or 3 × 10^5 luciferase-expressing Braf^{V600E}-induced melanoma cells (Cells) in the tail vein. Results are for 15 mice in each group; lungs were removed 27–32 days postinjection. Lower quartile, median, and upper quartile are shown, with whiskers extending to the lowest and highest values.

(D) Photomicrograph of metastatic melanoma deposit in the lung of a recipient mouse. Scale bar = 500 μm.

(E) Kaplan-Meier plots showing disease-free progression of study mice. The TM-treated *Braf$^{+/V600E}$;Tyr::CreERT2$^{+/o}$;p16$^{+/+}$* (V/E;Cre;p16 WT) group contained 28 animals, the TM-treated *Braf$^{+/V600E}$;Tyr::CreERT2$^{+/o}$;p16$^{-/-}$* (V/E;Cre;p16 null) group contained 10 animals, and controls included 8 *Braf$^{+/V600E}$;Tyr::CreERT2$^{+/o}$;p16$^{-/-}$* (V/E;Cre;p16 null) vehicle-treated or untreated animals. Additional controls are described in Table 2.

(F) Photograph showing nevi on the back of a TM-treated *Braf$^{+/V600E}$;Tyr::CreERT2$^{+/o}$;p16$^{INK4a-/-}$* mouse. The fur has been removed to reveal the lesions.

(G) *p16^{INK4a}* (p16) and *Gapdh* expression in skin harboring nevi or in tumors or liver from Braf^{V600E}-expressing mice. Skin from a wild-type mouse (WT skin) served as a negative control.

(H) p16^{INK4a} protein expression in Braf^{V600E}-induced tumors in *p16$^{INK4a+/+}$* (left) and *p16$^{INK4a-/-}$* (right) mice. Sections were counterstained with hematoxylin. Scale bar = 50 μm.

full transformation, so the cells become senescent and form a nevus. Eventually, some cells escape this senescence and progress to form a tumor, presumably through acquisition of additional mutations or genetic events. Although blue nevi were common at the periphery of the melanomas in our mice (Figures 4B and 4C) and nevus remnants in contiguity with melanomas have been described in 26%–85% of human nevi (Bevona et al., 2003; Greene et al., 1985), it is not possible to formally prove whether the tumors in our mice emerged directly out of nevi or whether they developed de novo.

Our data also suggest that Braf^{V600E} is more efficient at inducing melanoma than oncogenic Ras. With Braf^{V600E}, 11% of mice (3 of 28) developed melanoma within 6 months, rising to 54% within a year and 64% within 14 months. Hras^{G12V} induced melanoma in 3% of mice (1 of 41) in 6 months in one study (Chin et al., 1997) but did not induce melanoma at all in up to 8 months in another (Huijbers et al., 2006). Nras^{Q61K} induced melanoma in 28% of mice (4 of 14) within a year (Ackermann et al., 2005). These data reflect clinical experience in humans, where *BRAF* mutations are three times more common than *RAS* mutations (Garnett and Marais, 2004). However, the apparent increased potency of Braf^{V600E} may reflect differences in transgene design and oncogene expression levels rather than true biological differences between Braf^{V600E} and oncogenic Ras. This will need to be fully tested as more physiological models of melanoma using oncogenic Ras are developed.

The Braf^{V600E}-induced lesions we observed present an interesting paradox because blue nevi are comparatively rare in humans and do not generally harbor *BRAF* mutations (Yazdi et al., 2003). The predominance of dermal lesions in the Braf^{V600E} mice compared to humans may occur because melanocytes are predominantly dermal and rarely epidermal in mice, whereas the inverse is true in human skin (Hirobe, 1992). Nevertheless, the Braf^{V600E} tumors in our mice bear many characteristics of human oligomelanotic melanoma, including classic histological features such as nuclear pseudoinclusions and, although rare, pigmented neoplastic cells. We did not observe any evidence of metastasis in our mice. However, given the presence of ulceration, asymmetry, overt destructive growth patterns, and atypical cells with conspicuous nuclear pleomorphism (Figure 5A), histological features that are predictive of malignant behavior and metastatic potential in human melanoma, the Braf^{V600E}-induced tumors are likely to have metastatic potential. In support of this hypothesis, we have demonstrated that the tumor cells from these lesions can colonize the lungs of recipient mice when injected via the tail vein (Figures 5B–5E). Taken together, these data provide strong evidence of the metastatic potential of these oligomelanotic melanomas.

Table 2. Control Groups of Experimental Mice

Genotype	Phenotype	Treatment	Disease-free after 12 Months
$Braf^{+/LSL\text{-}V600E}$;$Tyr::CreERT2^{+/o}$;$p16^{INK4a+/+}$	$Braf^{V600E}$/CreERT2/$p16^{WT}$	untreated	8/8
$Braf^{+/+}$;$Tyr::CreERT2^{+/o}$;$p16^{+/+}$	$Braf^{WT}$/CreERT2/$p16^{WT}$	treated	14/14
$Braf^{+/LSL\text{-}V600E}$;$Tyr::CreERT2^{o/o}$;$p16^{+/+}$	$Braf^{V600E}$/$p16^{WT}$	treated	6/6
$Braf^{+/+}$;$Tyr::CreERT2^{o/o}$;$p16^{+/+}$	$Braf^{WT}$/$p16^{WT}$	treated	5/5
$Braf^{+/LSL\text{-}V600E}$;$Tyr::CreERT2^{+/o}$;$p16^{-/-}$	$Braf^{V600E}$/CreERT2/$p16^{null}$	untreated	8/8
$Braf^{+/+}$;$Tyr::CreERT2^{+/o}$;$p16^{-/-}$	$Braf^{WT}$/CreERT2/$p16^{null}$	treated	5/5
$Braf^{+/LSL\text{-}V600E}$;$Tyr::CreERT2^{o/o}$;$p16^{-/-}$	$Braf^{V600E}$/$p16^{null}$	treated	4/4

Untreated controls were either untreated or treated with vehicle (ethanol) only. Treated controls were treated with tamoxifen as described for experimental groups.

We investigated the role of $p16^{INK4a}$ in these $Braf^{V600E}$-induced tumors because metastatic lesions are seen in $Nras^{Q61K}$-induced melanomas in *p16*^{INK4a} null mice (Ackermann et al., 2005). Loss of $p16^{INK4a}$ did not augment metastatic behavior in the $Braf^{V600E}$-induced melanomas. However, we did find that although $p16^{INK4a}$ was upregulated in $Braf^{V600E}$-induced nevi (Figure 5H), *p16*^{INK4a} null mice still developed nevi (Figure 5G). We also found that nuclear $p16^{INK4a}$ was expressed in $Braf^{V600E}$-induced melanomas (Figure 5I). These observations appear counterintuitive since increased expression of *p16*^{INK4a} is a marker of senescence that is thought to provide protection from melanoma progression, and its loss is perceived to be an important step in melanomagenesis (Bennett, 2003). However, our findings are consistent with the clinical observations in humans. First, patients who carry mutations in both *CDKN2A* alleles and fail to express functional $p16^{INK4a}$ still develop nevi (Pavel et al., 2003). Second, although *p16*^{INK4a} is lost in most melanoma cell lines (Kamb et al., 1994), it is less commonly lost in clinical samples of melanoma. Thus, although early studies reported *p16*^{INK4a} mutations in 85% of familial melanoma cases (Gruis et al., 1995), larger population-based studies have reported mutation rates of 8%–40% (Goldstein et al., 2007; Holland et al., 1999; Ruiz et al., 1999). Furthermore, in sporadic melanoma, fewer than 2% of cases have mutations that affect *p16*^{INK4a} (Aitken et al., 1999; Orlow et al., 2007). Nuclear $p16^{INK4a}$ staining is still seen in 30%–85% of primary melanomas (Sanki et al., 2007; Sirigu et al., 2006), persists in microinvasive disease (Tuthill and Reed, 2007), and is reported in 15% of metastatic melanoma lesions (Sanki et al., 2007).

Thus, in accord with human physiology, although $p16^{INK4a}$ is upregulated in senescent mouse melanocytes, it is not required for the senescence response. Consequently, although $p16^{INK4a}$ is a tumor suppressor and a marker of senescence, it is not essential for nevus formation, and in agreement with human studies (Michaloglou et al., 2005), we conclude that $Braf^{V600E}$-mediated oncogene-induced senescence is independent of $p16^{INK4a}$. This suggests that other genes must contribute to, or be responsible for mediating, this response in melanocytes. Also in accord with human physiology, we have shown that $p16^{INK4a}$ loss is not essential for melanoma progression, although it does appear to regulate disease latency and penetrance.

In summary, we have developed a mouse model of melanoma driven by oncogenic Braf. The tumors we observed mimic those of amelanotic/oligomelanotic malignant metastatic melanoma in humans and are driven by a single human-relevant oncogene expressed at physiological levels. We have established that oncogenic Braf can induce melanocyte senescence in vivo and that *Braf* mutations can be founder genetic lesions in melanomagenesis. The long latency required for the development of melanoma demonstrates that oncogenic Braf alone is not sufficient to induce melanoma and that additional genetic lesions are required. The model we present here will play an important role in identifying those lesions.

EXPERIMENTAL PROCEDURES

Experimental Animals and Genotyping

Animal experiments were carried out under Home Office license authority in accordance with United Kingdom Coordinating Committee on Cancer Research guidelines (Workman et al., 1988) and with approval of the local Ethics Committee. Generation and genotyping of transgenic animals has been described previously (Mercer et al., 2005; Yajima et al., 2006). Tamoxifen (Sigma T5648) was freshly prepared in 100% ethanol. For tail vein injections, tumor cell lines were established by collecting tumors in sterile PBS, transferring them to DMEM/10% FCS and Primocin (0.1 mg/ml; InvivoGen), and dissociating them mechanically. Cells were allowed to attach to standard tissue culture plastic for 7 days, and clonal lines were derived by limiting dilution. Where appropriate, cells were treated with 300 pM cholera toxin (dissolved in PBS) or left untreated for 48 hr. For intravital imaging, cells were engineered to express firefly luciferase by transfection with the vector pMCEF-luciferase for clonal selection in G481 (4 mg/ml in DMEM/10% FCS). Tumor cells expressing luciferase (3×10^5 cells in 100 ml PBS) were injected into the tail vein of nude (NCr-nu) mice. Control mice received PBS. For intravital imaging, mice received intraperitoneal injections of D-luciferin in water (150 mg/kg body weight) 10 min before imaging. The animals were anesthetized with isoflurane, and tumors were imaged in an IVIS 100 (Xenogen), collecting data for 1 min for analysis with Living Image software.

Histology and Immunohistochemistry

Tumors were fixed in 10% buffered formalin and embedded in paraffin. Immunohistochemistry was performed on 3–10 μm sections stained with hematoxylin and eosin using standard protocols. $p16^{INK4a}$ antigen was retrieved by microwave (18 min in citrate buffer) and detection with rabbit polyclonal antibody ($p16^{INK4a}$; Santa Cruz, 1:50) and a Vectastain Elite ABC kit (Vector Laboratories) according to the manufacturer's instructions. For S100 and Ki-67 staining, antigen retrieval was performed in citrate buffer (pH 6.0, 30 min). S100 staining was revealed using a rabbit polyclonal antibody (Dako, 1:1000), a Rabbit enVision Peroxidase kit, and the AEC substrate chromogen (Dako). Ki-67 staining was revealed using a rat monoclonal antibody (Dako, 1:25), a rat Vectastain ABC kit (Vector Laboratories), and DAB as chromogen. Sections were counterstained with Harris's hematoxylin. Samples were stained for senescence-associated β-galactosidase as described previously (Gray-Schopfer et al., 2006). For bleaching prior to staining, sections were incubated in 0.1% $KMnO_4$ (20 min) followed by 0.5% oxalic acid (12 min).

DNA/RNA Techniques

DNA and RNA were extracted from snap-frozen tissues or cells using DNeasy and RNeasy kits, respectively (QIAGEN). First-strand cDNA synthesis from RNA was performed with 500 ng of total RNA and random hexanucleotides. For RT-PCR, specific genes were amplified under conditions in which amplification was still linear. Primer sequences are listed in the Supplemental Experimental Procedures.

SUPPLEMENTAL DATA

The Supplemental Data include Supplemental Experimental Procedures and three figures and can be found with this article online at http://www.cancercell.org/supplemental/S1535-6108(09)00074-9.

ACKNOWLEDGMENTS

This work was funded by Cancer Research UK (ref C107/A10433) and The Institute of Cancer Research. J.S.R.-F. and K.S. are funded by Breakthrough Breast Cancer. V.D. and L.L. are supported by Cancéropôle Île-de-France. We acknowledge National Health Service funding to the National Institute for Health Research Biomedical Research Centre.

Received: August 21, 2008
Revised: January 8, 2009
Accepted: February 24, 2009
Published: April 6, 2009

REFERENCES

Ackermann, J., Frutschi, M., Kaloulis, K., McKee, T., Trumpp, A., and Beermann, F. (2005). Metastasizing melanoma formation caused by expression of activated N-RasQ61K on an INK4a-deficient background. Cancer Res. *65*, 4005–4011.

Aitken, J., Welch, J., Duffy, D., Milligan, A., Green, A., Martin, N., and Hayward, N. (1999). CDKN2A variants in a population-based sample of Queensland families with melanoma. J. Natl. Cancer Inst. *91*, 446–452.

Bennett, D.C. (2003). Human melanocyte senescence and melanoma susceptibility genes. Oncogene *22*, 3063–3069.

Bevona, C., Goggins, W., Quinn, T., Fullerton, J., and Tsao, H. (2003). Cutaneous melanomas associated with nevi. Arch. Dermatol. *139*, 1620–1624.

Broome Powell, M., Gause, P.R., Hyman, P., Gregus, J., Lluria-Prevatt, M., Nagle, R., and Bowden, G.T. (1999). Induction of melanoma in TPras transgenic mice. Carcinogenesis *20*, 1747–1753.

Carr, S., See, J., Wilkinson, B., and Kossard, S. (1997). Hypopigmented common blue nevus. J. Cutan. Pathol. *24*, 494–498.

Chin, L., Pomerantz, J., Polsky, D., Jacobson, M., Cohen, C., Cordon-Cardo, C., Horner, J.W., 2nd, and DePinho, R.A. (1997). Cooperative effects of INK4a and ras in melanoma susceptibility in vivo. Genes Dev. *11*, 2822–2834.

Chin, L., Tam, A., Pomerantz, J., Wong, M., Holash, J., Bardeesy, N., Shen, Q., O'Hagan, R., Pantginis, J., Zhou, H., et al. (1999). Essential role for oncogenic Ras in tumor maintenance. Nature *400*, 468–472.

Garnett, M.J., and Marais, R. (2004). Guilty as charged: B-RAF is a human oncogene. Cancer Cell *6*, 313–319.

Goldstein, A.M., Chan, M., Harland, M., Hayward, N.K., Demenais, F., Bishop, D.T., Azizi, E., Bergman, W., Bianchi-Scarra, G., Bruno, W., et al. (2007). Features associated with germline CDKN2A mutations: a GenoMEL study of melanoma-prone families from three continents. J. Med. Genet. *44*, 99–106.

Gray-Schopfer, V.C., Cheong, S.C., Chong, H., Chow, J., Moss, T., Abdel-Malek, Z.A., Marais, R., Wynford-Thomas, D., and Bennett, D.C. (2006). Cellular senescence in naevi and immortalisation in melanoma: a role for p16? Br. J. Cancer *95*, 496–505.

Greene, M.H., Clark, W.H., Jr., Tucker, M.A., Elder, D.E., Kraemer, K.H., Guerry, D., 4th, Witmer, W.K., Thompson, J., Matozzo, I., and Fraser, M.C. (1985). Acquired precursors of cutaneous malignant melanoma. The familial dysplastic nevus syndrome. N. Engl. J. Med. *312*, 91–97.

Groben, P.A., Harvell, J.D., and White, W.L. (2000). Epithelioid blue nevus: neoplasm Sui generis or variation on a theme? Am. J. Dermatopathol. *22*, 473–488.

Gruis, N.A., van der Velden, P.A., Sandkuijl, L.A., Prins, D.E., Weaver-Feldhaus, J., Kamb, A., Bergman, W., and Frants, R.R. (1995). Homozygotes for CDKN2 (p16) germline mutation in Dutch familial melanoma kindreds. Nat. Genet. *10*, 351–353.

Hayward, N. (2000). New developments in melanoma genetics. Curr. Oncol. Rep. *2*, 300–306.

Hingorani, S.R., Jacobetz, M.A., Robertson, G.P., Herlyn, M., and Tuveson, D.A. (2003). Suppression of BRAF(V599E) in human melanoma abrogates transformation. Cancer Res. *63*, 5198–5202.

Hirobe, T. (1992). Control of melanocyte proliferation and differentiation in the mouse epidermis. Pigment Cell Res. *5*, 1–11.

Hoeflich, K.P., Gray, D.C., Eby, M.T., Tien, J.Y., Wong, L., Bower, J., Gogineni, A., Zha, J., Cole, M.J., Stern, H.M., et al. (2006). Oncogenic BRAF is required for tumor growth and maintenance in melanoma models. Cancer Res. *66*, 999–1006.

Holland, E.A., Schmid, H., Kefford, R.F., and Mann, G.J. (1999). CDKN2A (P16(INK4a)) and CDK4 mutation analysis in 131 Australian melanoma probands: effect of family history and multiple primary melanomas. Genes Chromosomes Cancer *25*, 339–348.

Huijbers, I.J., Krimpenfort, P., Chomez, P., van der Valk, M.A., Song, J.Y., Inderberg-Suso, E.M., Schmitt-Verhulst, A.M., Berns, A., and Van den Eynde, B.J. (2006). An inducible mouse model of melanoma expressing a defined tumor antigen. Cancer Res. *66*, 3278–3286.

Indra, A.K., Warot, X., Brocard, J., Bornert, J.M., Xiao, J.H., Chambon, P., and Metzger, D. (1999). Temporally-controlled site-specific mutagenesis in the basal layer of the epidermis: comparison of the recombinase activity of the tamoxifen-inducible Cre-ER(T) and Cre-ER(T2) recombinases. Nucleic Acids Res. *27*, 4324–4327.

Izquierdo, M.J., Pastor, M.A., Carrasco, L., Moreno, C., Kutzner, H., Sangueza, O.P., and Requena, L. (2001). Epithelioid blue naevus of the genital mucosa: report of four cases. Br. J. Dermatol. *145*, 496–501.

Kamb, A., Gruis, N.A., Weaver-Feldhaus, J., Liu, Q., Harshman, K., Tavtigian, S.V., Stockert, E., Day, R.S., 3rd, Johnson, B.E., and Skolnick, M.H. (1994). A cell cycle regulator potentially involved in genesis of many tumor types. Science *264*, 436–440.

Kannan, K., Sharpless, N.E., Xu, J., O'Hagan, R.C., Bosenberg, M., and Chin, L. (2003). Components of the Rb pathway are critical targets of UV mutagenesis in a murine melanoma model. Proc. Natl. Acad. Sci. USA *100*, 1221–1225.

Karasarides, M., Chiloeches, A., Hayward, R., Niculescu-Duvaz, D., Scanlon, I., Friedlos, F., Ogilvie, L., Hedley, D., Martin, J., Marshall, C.J., et al. (2004). B-RAF is a therapeutic target in melanoma. Oncogene *23*, 6292–6298.

King, R., Busam, K., and Rosai, J. (1999). Metastatic malignant melanoma resembling malignant peripheral nerve sheath tumor: report of 16 cases. Am. J. Surg. Pathol. *23*, 1499–1505.

Krimpenfort, P., Quon, K.C., Mooi, W.J., Loonstra, A., and Berns, A. (2001). Loss of p16Ink4a confers susceptibility to metastatic melanoma in mice. Nature *413*, 83–86.

Mercer, K., Giblett, S., Green, S., Lloyd, D., DaRocha Dias, S., Plumb, M., Marais, R., and Pritchard, C. (2005). Expression of endogenous oncogenic V600EB-raf induces proliferation and developmental defects in mice and transformation of primary fibroblasts. Cancer Res. *65*, 11493–11500.

Michaloglou, C., Vredeveld, L.C., Soengas, M.S., Denoyelle, C., Kuilman, T., van der Horst, C.M., Majoor, D.M., Shay, J.W., Mooi, W.J., and Peeper, D.S. (2005). BRAFE600-associated senescence-like cell cycle arrest of human naevi. Nature *436*, 720–724.

Moreno, C., Requena, L., Kutzner, H., de la Cruz, A., Jaqueti, G., and Yus, E.S. (2000). Epithelioid blue nevus: a rare variant of blue nevus not always associated with the Carney complex. J. Cutan. Pathol. *27*, 218–223.

Ohsie, S.J., Sarantopoulos, G.P., Cochran, A.J., and Binder, S.W. (2008). Immunohistochemical characteristics of melanoma. J. Cutan. Pathol. *35*, 433–444.

O'Keefe, E., and Cuatrecasas, P. (1974). Cholera toxin mimics melanocyte stimulating hormone in inducing differentiation in melanoma cells. Proc. Natl. Acad. Sci. USA *71*, 2500–2504.

Orlow, I., Begg, C.B., Cotignola, J., Roy, P., Hummer, A.J., Clas, B.A., Mujumdar, U., Canchola, R., Armstrong, B.K., Kricker, A., et al. (2007). CDKN2A germline mutations in individuals with cutaneous malignant melanoma. J. Invest. Dermatol. *127*, 1234–1243.

Patton, E.E., Widlund, H.R., Kutok, J.L., Kopani, K.R., Amatruda, J.F., Murphey, R.D., Berghmans, S., Mayhall, E.A., Traver, D., Fletcher, C.D., et al. (2005). BRAF mutations are sufficient to promote nevi formation and cooperate with p53 in the genesis of melanoma. Curr. Biol. *15*, 249–254.

Pavel, S., Smit, N.P., van der Meulen, H., Kolb, R.M., de Groot, A.J., van der Velden, P.A., Gruis, N.A., and Bergman, W. (2003). Homozygous germline mutation of CDKN2A/p16 and glucose-6-phosphate dehydrogenase deficiency in a multiple melanoma case. Melanoma Res. *13*, 171–178.

Pollock, P.M., Harper, U.L., Hansen, K.S., Yudt, L.M., Stark, M., Robbins, C.M., Moses, T.Y., Hostetter, G., Wagner, U., Kakareka, J., et al. (2003). High frequency of BRAF mutations in nevi. Nat. Genet. *33*, 19–20.

Powell, M.B., Hyman, P., Bell, O.D., Balmain, A., Brown, K., Alberts, D., and Bowden, G.T. (1995). Hyperpigmentation and melanocytic hyperplasia in transgenic mice expressing the human T24 Ha-ras gene regulated by a mouse tyrosinase promoter. Mol. Carcinog. *12*, 82–90.

Ruiz, A., Puig, S., Malvehy, J., Lazaro, C., Lynch, M., Gimenez-Arnau, A.M., Puig, L., Sanchez-Conejo, J., Estivill, X., and Castel, T. (1999). CDKN2A mutations in Spanish cutaneous malignant melanoma families and patients with multiple melanomas and other neoplasia. J. Med. Genet. *36*, 490–493.

Sanki, A., Li, W., Colman, M., Karim, R.Z., Thompson, J.F., and Scolyer, R.A. (2007). Reduced expression of p16 and p27 is correlated with tumor progression in cutaneous melanoma. Pathology *39*, 551–557.

Sirigu, P., Piras, F., Minerba, L., Murtas, D., Maxia, C., Colombari, R., Corbu, A., Perra, M.T., and Ugalde, J. (2006). Prognostic prediction of the immunohistochemical expression of p16 and p53 in cutaneous melanoma: a comparison of two populations from different geographical regions. Eur. J. Histochem. *50*, 191–198.

Tuthill, R.J., and Reed, R.J. (2007). Failure of senescence in the dysplasia-melanoma sequence: demonstration using a tissue microarray and a revised paradigm for melanoma. Semin. Oncol. *34*, 467–475.

Wellbrock, C., Ogilvie, L., Hedley, D., Karasarides, M., Martin, J., Niculescu-Duvaz, D., Springer, C.J., and Marais, R. (2004). V599EB-RAF is an oncogene in melanocytes. Cancer Res. *64*, 2338–2342.

Workman, P., Balmain, A., Hickman, J.A., McNally, N.J., Rohas, A.M., Mitchison, N.A., Pierrepoint, C.G., Raymond, R., Rowlatt, C., Stephens, T.C., et al. (1988). UKCCCR guidelines for the welfare of animals in experimental neoplasia. Lab. Anim. *22*, 195–201.

Yajima, I., Belloir, E., Bourgeois, Y., Kumasaka, M., Delmas, V., and Larue, L. (2006). Spatiotemporal gene control by the Cre-ERT2 system in melanocytes. Genesis *44*, 34–43.

Yazdi, A.S., Palmedo, G., Flaig, M.J., Puchta, U., Reckwerth, A., Rutten, A., Mentzel, T., Hugel, H., Hantschke, M., Schmid-Wendtner, M.H., et al. (2003). Mutations of the BRAF gene in benign and malignant melanocytic lesions. J. Invest. Dermatol. *121*, 1160–1162.

Zembowicz, A., Carney, J.A., and Mihm, M.C. (2004). Pigmented epithelioid melanocytoma: a low-grade melanocytic tumor with metastatic potential indistinguishable from animal-type melanoma and epithelioid blue nevus. Am. J. Surg. Pathol. *28*, 31–40.